J. Fluid Mech. (2013), *vol.* 720, *pp.* 192–211.
doi:10.1017/jfm.2013.24

Investigation of sub-Kolmogorov inertial particle pair dynamics in turbulence using novel satellite particle simulations

Baidurja Ray and Lance R. Collins†

Sibley School of Mechanical and Aerospace Engineering, Cornell University, Ithaca, NY 14850, USA

(Received 6 July 2012; revised 4 December 2012; accepted 5 January 2013;
first published online 27 February 2013)

Clustering (or preferential concentration) of weakly inertial particles suspended in a homogeneous isotropic turbulent flow is driven primarily by the smallest eddies at the so-called Kolmogorov scale. In particle-laden large-eddy simulations (LES), these small scales are not resolved by the grid and hence their effect on both the resolved flow scales and the particle motion have to be modelled. In order to predict clustering in a particle-laden LES, it is crucial that the subgrid model for the particles captures the mechanism by which the subgrid scales affect the particle motion (Ray & Collins, *J. Fluid Mech.*, vol. 680, 2011, pp. 488–510). In this paper, we describe novel satellite particle simulations (SPS), in which we study the clustering and relative velocity statistics of inertial particles at separation distances well below the Kolmogorov length scale. SPS is designed to isolate pairwise interactions of particles, and is therefore well suited for developing two-particle models. We show that the power-law dependence of the radial distribution function (RDF), a statistical measure of clustering, is predicted by the SPS in excellent agreement with direct numerical simulations (DNS) for Stokes numbers up to 3, implying that no explicit information from the inertial range is required to accurately describe particle clustering. This result further explains our successful prediction of the RDF power using the drift-diffusion model of Chun *et al.* (*J. Fluid Mech.*, vol. 536, 2005, pp. 219–251) for $St \leqslant 0.4$. We also consider the second-order longitudinal relative velocity structure function for the particles; we show that the SPS is able to capture its power-law exponent for $St \leqslant 0.5$ and attribute the disagreement at larger St to the effect of the larger scales of motion not captured by the SPS. Further, the SPS is able to capture the 'caustic activation' of the structure function at zero separation and predict the critical St and rate of activation in agreement with the DNS (Salazar & Collins, *J. Fluid. Mech.*, vol. 696, 2012, pp. 45–66). We show comparisons between filtered DNS and equivalently filtered SPS, and the findings are similar to the unfiltered case. Overall, SPS is an efficient and accurate computational tool for investigating particle pair dynamics at small separations, as well as an interesting platform for developing LES subgrid models designed to accurately reproduce particle clustering.

Key words: isotropic turbulence, multiphase and particle-laden flows, turbulence simulation

† Email address for correspondence: lc246@cornell.edu

1. Introduction

Inertial particles in turbulence have been shown to cluster outside of vortices, in the high-strain regions of the flow, using both numerical simulations (Maxey 1987; Squires & Eaton 1991; Wang & Maxey 1993; Eaton & Fessler 1994; Sundaram & Collins 1997) and experiments (Fessler, Kulick & Eaton 1994; Salazar *et al.* 2008; Saw *et al.* 2008; Gibert, Xu & Bodenschatz 2012). Such clustering can influence a broad range of aerosol processes, such as particle settling (e.g. Wang & Maxey 1993), evaporation and condensation (e.g. Shaw *et al.* 1998) and interparticle collisions (e.g. Sundaram & Collins 1997). It has been hypothesized that particle clustering plays a crucial role in the broadening of the droplet size distribution during both condensational growth and growth by collision and coalescence in warm cumulus clouds (Pinsky & Khain 1997; Shaw *et al.* 1998; Reade & Collins 2000*a*,*b*; Falkovich *et al.* 2002; Shaw 2003; Devenish *et al.* 2012; Grabowski & Wang 2012).

The radial distribution function (RDF) (McQuarrie 1976) has been established as a measure of particle clustering in isotropic turbulence and is defined as the ratio of the number of particle pairs found at a given separation distance to the expected number if the particles were uniformly distributed. The RDF can be computed from a field of M particles by binning the particles according to their separation distance and calculating

$$g(r_i) = \frac{N_{p,i}/\Delta V_i}{N_p/V}, \tag{1.1}$$

where $N_{p,i}$ is the average number of particles found in an elemental shell volume ΔV_i at a distance r_i from a test particle, V is the total volume and $N_p = M(M-1)/2$ is the total number of particle pairs in the flow. Sundaram & Collins (1997) showed that the RDF evaluated at particle contact precisely corrects the collision kernel for particle clustering. The average collision frequency for a monodisperse particulate system is given by

$$N_c = \frac{n^2}{2} K(\sigma), \tag{1.2a}$$

where σ denotes the particle diameter, $n \equiv M/V$ is the particle number density and $K(\sigma)$ is the collision kernel, defined for a statistically stationary suspension as

$$K(\sigma) = 4\pi\sigma^2 g(\sigma) \int_{-\infty}^{0} (-w_r) P(w_r|\sigma)\, \mathrm{d}w_r. \tag{1.2b}$$

As can be seen from (1.2*b*), apart from the RDF, the other statistical input to the collision kernel is the probability density function (p.d.f.) of the radial component of the relative velocity, w_r, defined as

$$w_r(\boldsymbol{r}) = [\boldsymbol{v}_2(\boldsymbol{x}+\boldsymbol{r}) - \boldsymbol{v}_1(\boldsymbol{x})] \cdot \frac{\boldsymbol{r}}{|\boldsymbol{r}|}, \tag{1.3}$$

where $\boldsymbol{v}_1(\boldsymbol{x})$ and $\boldsymbol{v}_2(\boldsymbol{x}+\boldsymbol{r})$ are the velocities of two particles located at $\boldsymbol{x}$ and $\boldsymbol{x}+\boldsymbol{r}$, respectively. The effect of inertia on the radial relative velocity statistics has been investigated in the context of predicting the collision kernel (Wang, Wexler & Zhou 2000; Ayala, Rosa & Wang 2008*a*; Ayala *et al.* 2008*b*; Bec *et al.* 2010; de Jong *et al.* 2010) and also for modelling the particle motion that leads to clustering (Chun *et al.* 2005; Zaichik & Alipchenkov 2009; Pan & Padoan 2010). Recently, it has been hypothesized that inertial particle relative velocities can be multi-valued in the limit of zero separation owing to the formation of caustics (Falkovich *et al.* 2002; Wilkinson,

Mehlig & Bezuglyy 2006; Falkovich & Pumir 2007; Salazar & Collins 2012), which, if they exist, would tend to enhance the collision rate.

It is apparent from (1.2*b*) that the collision kernel for asymptotically small particles (i.e. $\sigma/\eta \ll 1$) will depend sensitively on the near-contact concentration and motion of particle pairs. Direct numerical simulation (DNS) has proven effective for analysing the behaviour of these statistics as a function of the separation distance for small separations (i.e. $\Delta/\eta \ll 1$, where Δ is the smallest separation of interest); however, there are two fundamental challenges with DNS. Firstly, the number of particles required to achieve statistical convergence at a separation distance Δ scales like $M \sim N^3\,(\eta/\Delta)^3$, where N is the number of grid points in each direction. This scaling is challenging, given the desire to simultaneously explore higher Reynolds numbers (i.e. larger N) and smaller separation distances (i.e. larger η/Δ). Secondly, the near-contact motion of the particles will depend in some unknown way on the accuracy of the interpolation scheme used to obtain the fluid velocity at the particle centre, particularly at these small separations. There has not been a systematic study of how errors in spatial interpolation (and even time stepping) manifest in the scaling of these near-contact statistics.

We present an alternative framework called 'satellite particle simulations' (SPS). With SPS, we simulate a cloud of satellite particles surrounding each primary particle, assuming that the satellites are sufficiently close to the primary particle that a locally linear flow assumption can be made. The relative velocity of the fluid is then defined completely in terms of the fluid velocity gradient along the inertial (primary) particle trajectory. This quantity is obtained from the DNS. The dynamics of the satellite particles are therefore the dynamics of particle pairs in the asymptotic limit $\Delta/\eta \to 0$, thus overcoming the first concern discussed above. The locally linear flow assumption also eliminates the interpolation errors, and so SPS can be considered the most accurate description of near-contact motion of particle pairs possible. However, SPS has limitations as well. Firstly, because SPS contains no information about the inertial subrange, it cannot predict the entire behaviour of the position and velocity statistics. For example, the RDF is known to behave as a power law in the dissipation range (Reade & Collins 2000*a*; Kerstein & Krueger 2006) – SPS predicts the power, but not the prefactor, which depends upon both the dissipation and inertial subranges. Secondly, we have no precise means for specifying the velocity of incoming satellites entering the fluid volume. As a first approximation, we assign these particles the corresponding fluid velocities at their spatial locations. This approximation is exact in the limit $St \to 0$, and is expected to become less accurate as the particle inertia increases. These simulations, therefore, allow us to test whether (and how) particle clustering in the dissipation range (across a wide range of St) is influenced by information from the larger scales of the flow. More details about the SPS can be found in §§ 2.2 and 3.1.

In this paper, we compare DNS and SPS predictions of the RDF and the second-order velocity structure function. The velocity gradient required for the SPS was obtained from the same DNS, ensuring a fair comparison of the two methods. We make these comparisons over a wide range of particle Stokes numbers to quantify the effect of the error associated with the arbitrary boundary condition in the SPS. The results also shed light on the theoretical framework of Chun *et al.* (2005), which is based on the same locally linear flow assumption.

The second goal of the paper is to consider the effect of filtering on sub-Kolmogorov clustering using the SPS. This is motivated by our previous work (Ray & Collins 2011), where we used a filtered DNS (FDNS) as an *a priori* large-eddy

simulation (LES) (Fede & Simonin 2006) and established the effect of velocity filtering on the RDF and w_r across a wide range of St and r/η. In that paper, we concluded that, in order to capture particle clustering in an LES, we need to model the mechanism by which particles cluster at the subgrid scales. Recently, there has been considerable interest in particle-laden LES (Bini & Jones 2008; Marchioli, Salvetti & Soldati 2008; Jin, He & Wang 2010; Ray & Collins 2011), and various models have been put forward to capture the effect of the subgrid scales on particle motion. Shotorban & Mashayek (2005) and Kuerten (2006) used the approximate deconvolution method to model the resolved scales exactly, while Shotorban & Mashayek (2006*a*,*b*) considered a generalized Langevin-type model for fluid velocities 'seen' by inertial particles. However, these studies focused primarily on one-particle statistics such as the root mean-square (r.m.s.) velocity and displacement of the particles. In fact, attempts at predicting clustering via one-particle models (Pozorski & Apte 2009) suggest that they contain insufficient physics to capture a phenomenon that is essentially governed by two-particle dynamics. Our SPS provides a natural framework to investigate pairwise interaction between particles. The feasibility of using the SPS as a test-bed for two-particle LES models is tested by using a filtered SPS (FSPS) and comparing it with results from FDNS. We will show that the SPS indeed provides a valid test-bed for *a priori* testing of LES models.

This paper is organized as follows. In § 2.1 we describe the details of the numerical methods used to evolve the isotropic turbulent flow field and track a large number of inertial particles in it, spanning a wide range of St. Section 2.2 describes the concept and implementation of the SPS. Section 3 presents the results, beginning with the effect of the choice of R/η on the SPS in § 3.1. Sections 3.2 and 3.3 then compare the results of the RDF and the longitudinal relative velocity structure function for unfiltered and filtered DNS (and SPS), respectively. Section 4 provides some concluding remarks.

2. Numerical simulations

2.1. *Direct numerical simulation*

In this section, we present details of the DNS used to solve the three-dimensional time-dependent Navier–Stokes equations for the fluid phase with and without filtering, and the equations of motion for the inertial particles suspended in the fluid.

2.1.1. *Fluid phase*

The governing equations for a three-dimensional incompressible flow are the continuity and the Navier–Stokes equation. In rotational form, the equations are

$$\frac{\partial u_i}{\partial x_i} = 0, \tag{2.1}$$

$$\frac{\partial u_i}{\partial t} + \epsilon_{ijk}\omega_j u_k = -\frac{\partial (p/\rho + \frac{1}{2}u^2)}{\partial x_i} + \nu \frac{\partial^2 u_i}{\partial x_j \partial x_j}, \tag{2.2}$$

where u_i is the velocity vector, $u \equiv \sqrt{u_i u_i}$ is the magnitude of the velocity vector, ρ is the fluid density, ν is the kinematic viscosity, ϵ_{ijk} is the alternating unit tensor, ω_i is the vorticity and p is the pressure. In order to maintain a statistically stationary isotropic turbulence, we use a time-dependent deterministic forcing function that injects energy into the first two wavenumbers in Fourier space (Witkowska, Brasseur & Juvé 1997). Equations (2.1) and (2.2) are solved using a pseudo-spectral algorithm with de-aliasing based on a combination of truncation and phase shift (Patterson & Orszag 1971;

Variable	DNS	FDNS	SPS (FSPS)
N	128	128	—
R_λ	95	—	95
$\kappa_{max}\eta$	1.508	—	1.508
k	1.178	1.080	1.178 (1.080)
ϵ	0.232	0.085	0.232 (0.085)
η	0.025	—	0.025
τ_η	0.139	—	0.139
L	1.490	—	1.490
N_p	6 000 000	6 000 000	1 152 000
$\langle N_s \rangle$	—	—	300
R	—	—	0.6η, 2η

TABLE 1. Turbulence parameters for DNS, FDNS and SPS. Here N is the number of grid points in each of the three dimensions; R_λ is the Reynolds number based on the Taylor micro-scale; $k = \int_0^{\kappa_{max}} E(\kappa)\,\mathrm{d}\kappa$ is the kinetic energy; $\epsilon = 2\nu \int_0^{\kappa_{max}} \kappa^2 E(\kappa)\,\mathrm{d}\kappa$ is the dissipation rate; $\eta = \nu^{3/4}/\epsilon^{1/4}$ is the Kolmogorov length scale; $\tau_\eta = \sqrt{\nu/\epsilon}$ is the Kolmogorov time scale; $L = (3\pi/2k) \int_0^{\kappa_{max}} (E(\kappa)/\kappa)\,\mathrm{d}\kappa$ is the integral length scale; for FDNS, k and ϵ are computed by replacing κ_{max} by the cutoff filter scale κ_c; N_p is the total number of particles (primary particles in the case of SPS); $\langle N_s \rangle$ is the average number of satellite particles per primary particle; and R is the chosen outer sphere radius bounding the SPS domain.

Zemach 1998; Brucker *et al.* 2007) on a standard periodic cube of length 2π (in arbitrary units). We use 128 grid points in each direction, which yields $R_\lambda \approx 95$. This is smaller than earlier simulations (e.g. Ray & Collins 2011), but this allows us to achieve excellent convergence in both SPS and DNS at very small separations. This is especially relevant for SPS, which has the more demanding memory requirements (as each primary particle has a cloud of several hundred satellite particles that are tracked). Fortunately, previous studies have shown that at small separations the RDF and the relative velocity structure function are only weak functions of R_λ (Wang *et al.* 2000; Hogan & Cuzzi 2001; Collins & Keswani 2004; Ray & Collins 2011). Collins & Keswani (2004) analysed this dependence in detail for $St \leqslant 1.5$ and found that the sensitivity increased slightly with increasing Stokes number. More recently, Ray & Collins (2011) found a somewhat stronger dependence of the RDF on R_λ, but only for $St \geqslant 2.0$ (see figure 2*c* in that paper). We conclude that the present simulations at $R_\lambda = 95$ are sufficient for the purposes of comparing SPS and DNS at small separations. The time step for the fluid was chosen so that the Courant–Friedrichs–Levy (CFL) number is less than 0.5. We evolve the flow field for about 13 eddy turnover times to reach statistical stationarity. Additional details of simulation parameters and resolution are given in table 1.

2.1.2. *Filtering*

We perform low-pass filtering of the DNS velocity field in Fourier space so that all the Fourier modes of velocity beyond a certain cutoff wavenumber κ_c are removed from the flow and only the remaining 'large scales' are retained. The filtering operation we perform is defined below. We apply a sharp spectral filter that removes all wavenumbers above a critical wavenumber κ_c, yielding the following definition of

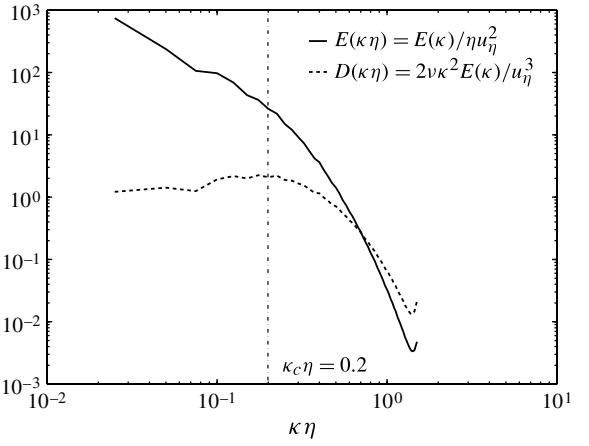

FIGURE 1. Filter cutoff scale ($\kappa_c\eta = 0.2$) superimposed on the energy ($E(\kappa)/\eta {u_\eta}^2$) and dissipation ($2\nu\kappa^2 E(\kappa)/{u_\eta}^3$) spectra. Notice that $\kappa_c\eta$ is within the inertial subrange.

the filtered velocity:

$$\tilde{\boldsymbol{u}}(\boldsymbol{k}, t) = \begin{cases} \boldsymbol{u}(\boldsymbol{k}, t) & \text{if } |\boldsymbol{k}| \leqslant \kappa_c, \\ \boldsymbol{0} & \text{otherwise,} \end{cases} \tag{2.3}$$

where we use a cutoff wavenumber $\kappa_c\eta = 0.2$. Figure 1 shows the energy and dissipation spectra obtained from our DNS as a function of wavenumber. Note that the cutoff wavenumber (or filter scale) lies within the inertial subrange. The turbulent kinetic energy and dissipation rate are computed for the filtered velocity field using the standard definitions shown in table 1, with κ_{max} replaced by κ_c. In Ray & Collins (2011), we showed that the statistics of interest vary monotonically as a function of κ_c in the inertial range, and therefore any value in that range can be used to evaluate the effect of filtering. It is worth noting that if we choose the cutoff wavenumber in the dissipation subrange, the filtering has very little effect on clustering.

2.1.3. *Inertial particle motion*

We assume a dilute suspension of inertial particles, which allows us to neglect the feedback of particle motion on the carrier fluid (Sundaram & Collins 1999). We also consider particles whose radius a is much smaller than the Kolmogorov length scale η and simulate them as point particles. Furthermore, we assume that the particles are much denser than the surrounding fluid ($\rho_p/\rho_f \gg 1$), the particle Reynolds numbers are small, and collisions and gravitational settling are neglected. Under these assumptions, the equations of motion for the particles reduce to (Maxey & Riley 1983)

$$\frac{\mathrm{d}\boldsymbol{x}(t)}{\mathrm{d}t} = \boldsymbol{v}(t), \tag{2.4}$$

$$\frac{\mathrm{d}\boldsymbol{v}(t)}{\mathrm{d}t} = \frac{\boldsymbol{u}[\boldsymbol{x}(t)] - \boldsymbol{v}(t)}{\tau_p}, \tag{2.5}$$

where $\boldsymbol{x}$ is the inertial particle position, $\boldsymbol{v}$ is the particle velocity, $\tau_p = (2/9)\rho_p a^2/\rho_f\nu$ is the particle response time and $\boldsymbol{u}(\boldsymbol{x})$ denotes the fluid velocity at the inertial particle location. We have used 1 152 000 particles (as primary particles for SPS) divided

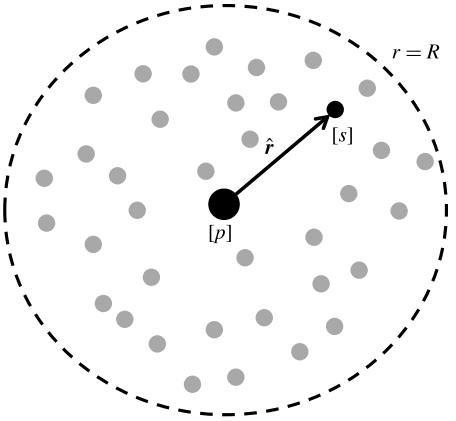

FIGURE 2. Illustration of the SPS: '[p]' denotes the primary particle, '[s]' denotes a satellite particle, $\hat{\boldsymbol{r}}$ is their separation vector and $r = R$ denotes the bounding sphere beyond which we no longer simulate the satellite particle motion.

equally into 12 different Stokes numbers. Since we need to compare the results from the SPS to those in the DNS at small separations, we have used 6 000 000 particles divided into 12 different St for the DNS (and FDNS) to obtain reliable statistics at the sub-Kolmogorov scales. These particles are introduced into the stationary flow field at random positions and with the fluid velocity at those locations. Particles are advanced in time according to (2.4) and (2.5) using an improved numerical scheme that was recently developed in our group (Ireland *et al.* 2012). This new algorithm, based on exponential integrators, is second-order accurate in time and can simulate particles with arbitrarily small St accurately, allowing us to use the fluid time step (dictated by the CFL condition) to advance the inertial particles, irrespective of St, thereby significantly reducing the run times for low-St particles. Fluid velocities at particle locations are obtained using eighth-order Lagrangian interpolation. We allow sufficient time (four eddy turnover times) for the particles to equilibrate with the flow before taking statistics. Particle statistics are averaged over several eddy turnover times. In order to investigate the effect of filtering, the particles are similarly advanced using the filtered velocity field.

2.2. *Satellite particle simulation*

We consider a reference frame moving with an inertial particle (henceforth referred to as a 'primary particle', denoted by a superscript '[p]') and simulate the motion of a cloud of surrounding particles (henceforth referred to as 'satellite particles', denoted by a superscript '[s]') with respect to the primary particle (see figure 2). Denoting the relative position and velocity of the satellite particles as $\hat{\boldsymbol{r}}$ and $\hat{\boldsymbol{w}}$, where $\hat{\boldsymbol{r}} = \boldsymbol{x}^{[s]} - \boldsymbol{x}^{[p]}$ and $\hat{\boldsymbol{w}} = \boldsymbol{v}^{[s]} - \boldsymbol{v}^{[p]}$, we use (2.4) and (2.5) to derive the equations of motion of a satellite particle as

$$\frac{\mathrm{d}\hat{\boldsymbol{r}}(t)}{\mathrm{d}t} = \hat{\boldsymbol{w}}(t), \tag{2.6}$$

$$\frac{\mathrm{d}\hat{\boldsymbol{w}}(t)}{\mathrm{d}t} = \frac{\Delta \boldsymbol{u}[\hat{\boldsymbol{r}}(t)] - \hat{\boldsymbol{w}}(t)}{\tau_p}, \tag{2.7}$$

where $\Delta\boldsymbol{u}[\hat{\boldsymbol{r}}(t)] \equiv \boldsymbol{u}[\boldsymbol{x}^{[s]}] - \boldsymbol{u}[\boldsymbol{x}^{[p]}]$, and we have assumed that the primary and satellite particles have the same response times (i.e. a monodisperse population of particles). Hereafter in this paper, we deliberately make a distinction between the phase-space variable $\boldsymbol{r}$ denoting the space of all possible values taken by the separation vector between particle pairs, and the Lagrangian time-dependent separation vector $\hat{\boldsymbol{r}}(t)$ between a satellite particle and its primary particle. This will be relevant primarily in the discussion of the drift-diffusion model based on the theory of Chun *et al.* (2005) in § 3.2.

The approach we take is to perform a traditional simulation of a population of primary particles using (2.4) and (2.5). Simultaneously, we evolve the relative position and velocity of the satellite particles surrounding each primary particle according to (2.6) and (2.7). Such a solution requires the relative fluid velocity $\Delta\boldsymbol{u}[\hat{\boldsymbol{r}}(t)]$. In general, this is very difficult to specify in a turbulent flow; however, since we are interested in separation distances below the Kolmogorov length scale (i.e. $\hat{r}/\eta < 1$), we can approximate the relative fluid velocity based on a locally linear flow assumption, i.e.

$$\Delta u_i[\hat{\boldsymbol{r}}(t)] = \Gamma_{ij}^{[p]}(t)\hat{r}_j, \tag{2.8}$$

where the Einstein summation convention is implied, and $\Gamma_{ij}^{[p]}(t) = \partial u_i^{[p]}(t)/\partial x_j$ is the velocity gradient at the primary particle location at time t. The task of specifying $\Delta\boldsymbol{u}$ now reduces to calculating $\Gamma_{ij}^{[p]}(t)$ along each *primary* particle trajectory in the DNS. We then have the information required to evolve (2.6) and (2.7). Note that $\Gamma_{ij}^{[p]}(t)$ could be obtained from a model such as the one by Chevillard & Meneveau (2006), which would eliminate the computational cost of performing the DNS, thereby drastically reducing the computational time for SPS.

We advance the particles following (2.6) and (2.7) using the second-order accurate exponential integrator defined in Ireland *et al.* (2012). However, this reduction in the phase space of the system generates another issue. Such a locally linear flow is applicable at small separations, but the satellite particles eventually diffuse beyond the satellite volume boundary at $r = R$ (see figure 2). To maintain a statistically stationary sample of particles in the satellite volume, we must provide an equal source of particles diffusing into the satellite volume. This inward flux is generated by introducing new satellite particles at the boundary. There is no precise way of specifying the initial conditions for these particles, so we place them at random on the bounding surface corresponding to $\hat{r} = R$ and set the particle velocity to the underlying fluid velocity at that location (based on the locally linear flow approximation). In addition, we need to ensure that the velocity of the newly created particle points inwards, i.e. $\hat{\boldsymbol{w}} \cdot \boldsymbol{n} < 0$, where $\hat{\boldsymbol{w}}$ is the velocity of the newly created particle relative to the primary particle and $\boldsymbol{n}$ is the outward normal to the surface of the sphere at the new particle location. We employ the following algorithm to create new (replacement) particles in an SPS (Ahluwalia 2002; Chun *et al.* 2005). We define a probability of creating new particles in a particular trial as

$$P_{creation} = \frac{-\hat{\boldsymbol{w}} \cdot \boldsymbol{n}}{|\hat{\boldsymbol{w}} \cdot \boldsymbol{n}|_{max}}, \tag{2.9}$$

where $|\hat{\boldsymbol{w}} \cdot \boldsymbol{n}|_{max} \approx 2R\langle\Gamma_{11}^2\rangle^{1/2} \approx 2R/\sqrt{15}\tau_\eta$. Then, we generate a uniform random number $X \in [0, 1)$, and at each trial create a new particle only if $P_{creation} > 0$ and $P_{creation} > X$. We expect the number of satellite particles leaving the bounding sphere at any instant of time to differ for each primary particle, making it necessary to define an average number of satellite particles per primary particle. For example, primary

particles lying in regions of high strain rate would be likely to contain more satellite particles than those lying in regions of high rotation rate. The above rule of thumb (2.9) generates $P_{creation} > 1$ for 2–3 % of the trials. In those cases, we create a particle and use the remaining probability $P_{creation} - 1$ to determine whether another particle should be created. By using the above algorithm, and selecting a fixed number of trials to create new particles (for each St), we can control the *average* number of satellite particles per primary particle. The quantity $\langle N_s \rangle$ in table 1 denotes the average number of satellite particles per primary particle at stationary state. Clearly, this boundary condition is artificial, and so we will need to determine the impact that this has on the accuracy of the SPS method. We expect the approximation to be accurate in the limit $St \to 0$, and to degrade with increasing Stokes number. Additional details on how to obtain statistics from our SPS are given below.

3. Results and discussion

We perform DNS and SPS in matched turbulent flows and with overlapping values of the particle Stokes numbers so that detailed comparisons can be made. In general, the RDF and the second-order longitudinal relative velocity structure function ($S_2 = \langle w_r^2 \rangle$) behave like power laws in the dissipation range, taking the form $g(r) \approx c_0 \, (\eta/r)^{c_1}$ (e.g. Reade & Collins 2000*a*) and $S_2 \approx a + b \, (r/\eta)^{\zeta_2}$ (Salazar & Collins 2012). As noted earlier, the prefactors c_0 and a, b involve the inertial subrange as well and hence are not determined quantitatively in the SPS. Therefore we focus the comparisons on the predicted powers c_1 and ζ_2, and on the qualitative behaviour of $a(St)$, which is known as the 'caustic' contribution to S_2. In an SPS, we compute particle statistics by directly binning the position of the satellite particles (which denotes the relative two-particle separation $\boldsymbol{r}$) and then averaging this over all primary particles. For example, if the number of satellite particles lying within radii $r_{i+1/2}$ and $r_{i-1/2}$ from a primary particle is $N_{s,i}$, and the total number of satellite particles within its bounding sphere is $N_{s,T}$, then the RDF would be computed as $g(r_i) = \langle N_{s,i}/(r_{i+1/2}^3 - r_{i-1/2}^3) \rangle / \langle N_{s,T}/R^3 \rangle$, where the average is over all the primary particles in the system (for a particular St). The results are further averaged over several Kolmogorov times, after achieving statistical stationarity. With SPS, the radius of the satellite shell volume, R, is arbitrary, introducing another parameter that we define as R/η. In addition to the significance of this parameter, which is discussed in § 3.1, the bounding surface also introduces some arbitrariness in setting the boundary conditions for particles entering the satellite volume. We expect the imprecision of the boundary conditions to contaminate the particle statistics close to the boundary. Empirically, we find that if we perform a least-squares fit of the RDF or relative velocity structure function, and limit the range of the fit to $r/R \leqslant 0.3$, the results are insensitive to the boundary conditions over the entire range of Stokes numbers in this study.

3.1. *SPS: effect of* R/η

To analyse the effect of the satellite volume radius, we performed SPS using $R/\eta = 0.6$ and 2.0. Figure 3(*a*) compares the RDFs plotted versus r/R for both values of R/η. Note that the two curves collapse on top of each other, indicating that the choice of R/η has no effect on the RDF plotted in this coordinate system. This is verified in figure 3(*b*), which shows that R/η has no effect on the power $c_1(St)$.

We also look at the effect of R/η on S_2. Figure 4(*a*) shows the variation of S_2 normalized by u_η^2 as a function of r/R for the same two R/η. In contrast to the RDF,

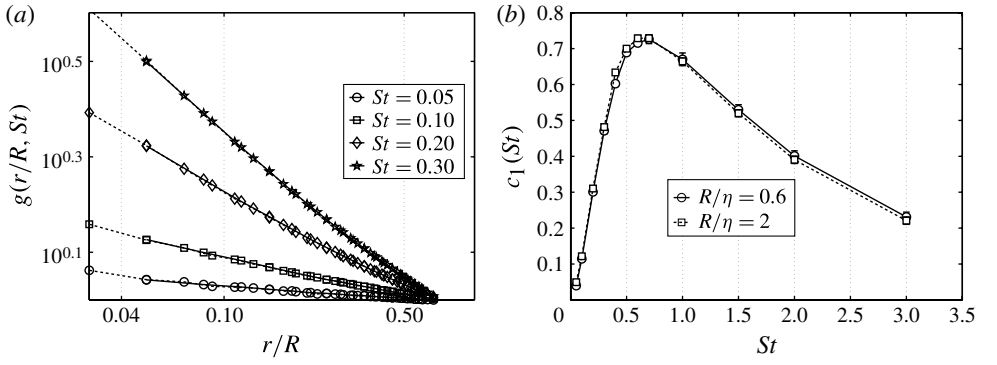

FIGURE 3. (*a*) Variation of the RDF predicted by the SPS as a function of r/R for four different St (0.05, 0.10, 0.20 and 0.30) and two different choices of R: solid line indicates $R = 0.6\eta$ and dashed line indicates $R = 2\eta$. (*b*) Variation of c_1 as a function of St for the two different choices of R. The error bars correspond to 95 % confidence intervals.

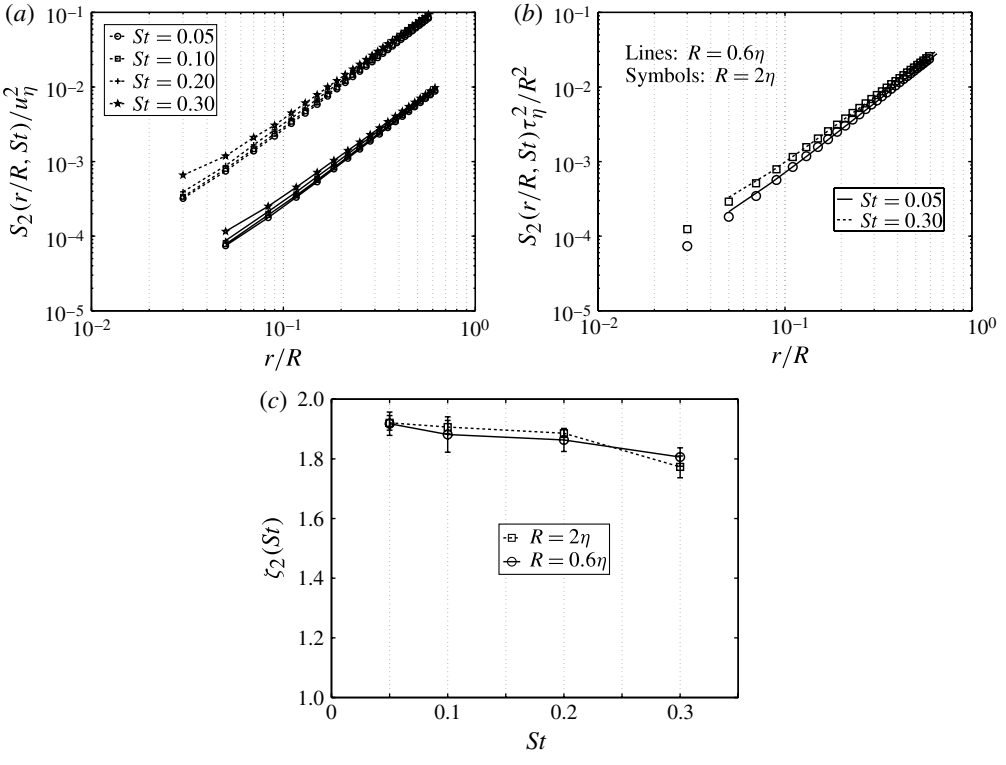

FIGURE 4. (*a*) The second-order longitudinal structure function S_2 as a function of r/R for $St = 0.05$, 0.10, 0.20 and 0.30 as indicated and for $R/\eta = 0.6$ (solid line) and 2.0 (dashed line). (*b*) Replotted S_2 normalized by $(R/\tau_\eta)^2$ as a function of r/R for $St = 0.05$ and 0.30 and for $R/\eta = 0.6$ (lines) and 2.0 (symbols). (*c*) Variation of ζ_2 as a function of St for the two values of R/η. Error bars correspond to 95 % confidence intervals.

the structure functions do not collapse in this coordinate. This is not surprising, as the magnitude of the velocity increases linearly with r and therefore the variance too should increase with increasing R/η. Taking this into consideration, figure 4(*b*) shows S_2 for $St = 0.05$ and 0.3 normalized by the factor $(R/\tau_\eta)^2$. The data for both R/η clearly collapse under this normalization. Furthermore, if we consider the exponent of the power law ζ_2, it is insensitive to R/η, as shown in figure 4(*c*).

We conclude that there are simple scalings that relate SPS with different R/η, and predictions of c_1 and ζ_2 are not affected by the choice of R/η.

3.2. *DNS versus SPS: unfiltered turbulence*

Now that we have established a basis for comparing DNS and SPS, we focus on comparisons for unfiltered turbulence. Before we begin, it is useful to review the theory of Chun *et al.* (2005), which, based on the same locally linear flow assumption as made in the SPS, derived the following closed differential equation for the RDF:

$$\frac{\partial g(r,t)}{\partial t} = \frac{1}{r^2}\frac{\partial [A(St) r^3 g(r,t)]}{\partial r} + \frac{1}{r^2}\frac{\partial}{\partial r}\left[B r^4 \frac{\partial g(r,t)}{\partial r}\right], \tag{3.1}$$

where $A(St)$ and B are the 'drift' and 'diffusion' coefficients, respectively. The steady-state solution of (3.1) takes the form $g(r/\eta) = c_0\,(r/\eta)^{-c_1}$, where $c_1 = A(St)/B$ and, as with SPS, c_0 is an undetermined parameter that depends on a boundary condition in the inertial subrange. The theory further predicts the mean inward drift velocity (in the absence of diffusion) to be

$$\langle \hat{w}_i(t) | \hat{r}_i(t) = r_i \rangle_p = -A(St) r_i, \tag{3.2}$$

where the drift coefficient (same as in (3.1)) is given by

$$A(St) = \frac{St}{3}(\langle S^2 \rangle_p - \langle R^2 \rangle_p)\tau_\eta. \tag{3.3}$$

Note that $\hat{\boldsymbol{r}}(t)$ is a *Lagrangian time-dependent* variable representing the separation vector between a satellite particle and its primary particle (distinguishable from the phase-space variable $\boldsymbol{r}$, as for example in (3.1)), $\langle \cdot \rangle_p$ denotes an average over all primary particle positions at time t, $\hat{w}_i(t)$ is the relative velocity of a satellite particle with respect to its primary particle, and $S(t)^2 = S_{ij}(t)S_{ij}(t)$ and $R(t)^2 = R_{ij}(t)R_{ij}(t)$ are the second invariants of the rate-of-strain and rate-of-rotation tensors at the primary particle location, respectively. Under statistical stationarity, $A(St)$ is not a function of time. Based on this drift-diffusion argument, Chun *et al.* (2005) conclude that particle pairs obeying the following relation should cluster like inertial particles

$$\frac{\mathrm{d}\hat{r}_i(t)}{\mathrm{d}t} = -A(St)\hat{r}_i(t) + \Gamma_{ij}(t)\hat{r}_j(t). \tag{3.4}$$

We will analyse this relation as well.

Figure 5(*a*) compares the variation of the RDF with r/η for the DNS and the SPS over a range of Stokes numbers. We can see that the qualitative behaviour is very similar. It should be noted that the value of r/η in an SPS has no physical meaning when compared to DNS, unless the boundary condition specified at $r = R$ is exact. We show the comparison in figure 5(*a*) (and some of the figures to follow) as a function of r/η for illustration purposes only. It is meaningful, however, to compare the power c_1, as obtained from a nonlinear least-squares fit of the RDF data for DNS and SPS. Figure 5(*b*) shows that they are nearly identical, to within

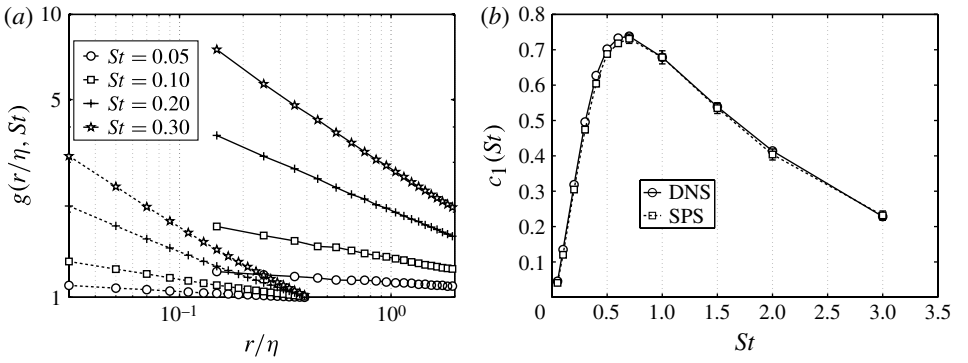

FIGURE 5. (*a*) Variation of the RDF as a function of r/η for four different St (0.05, 0.10, 0.20 and 0.30) in the DNS and SPS: solid line indicates DNS and dashed line indicates SPS. (*b*) Variation of c_1 as a function of St in the DNS and SPS. The error bars correspond to 95 % confidence intervals.

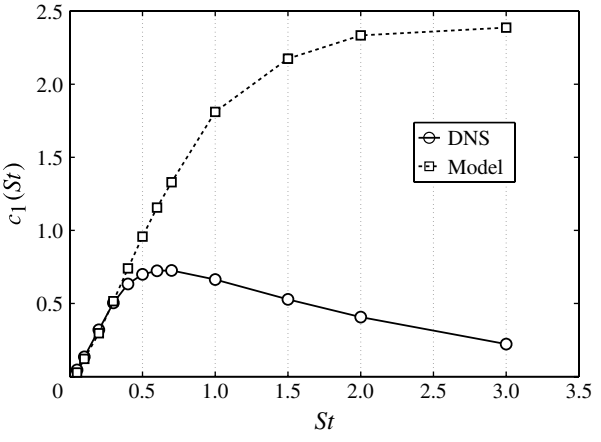

FIGURE 6. Variation of c_1 as a function of St predicted by the DNS and the model (3.4).

the 95 % confidence intervals for the fits. This remarkable agreement suggests that the outer flow information coming from the inertial subrange and beyond has very little to do with the power-law scaling of the RDF within the dissipation range over the entire range of Stokes numbers considered in this study. This important result supports theories like those by Chun *et al.* (2005) and Zaichik & Alipchenkov (2007) that are based on a similar local assumption.

According to the model shown in (3.4), the satellite particles drift inwards towards the primary particle with a velocity proportional to their separation, which is counteracted by a random diffusion term that is assumed to be given by the fluid velocity at the satellite particle position. We can test this model by advancing an ensemble of *fluid* particles as primary particles, each with a population of satellite particles obeying (3.4). In this model, all the information about particle inertia is embedded in the drift coefficient $A(St)$ defined in (3.3). The average values of the second invariants of the strain and rotation rates in $A(St)$ are required as inputs to the model and are computed from DNS. Figure 6 shows the comparison of c_1

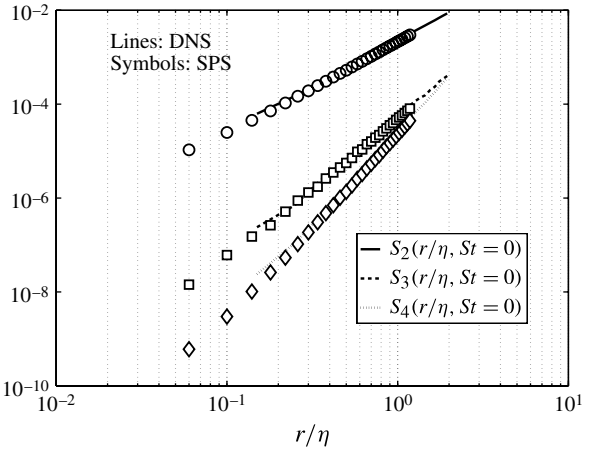

FIGURE 7. Comparison of longitudinal structure functions of order $p = 2, 3, 4$ for fluid particles in DNS (lines) and SPS (symbols).

obtained from the model and DNS. There is very good agreement for $St \leqslant 0.4$, supporting the low-Stokes-number analysis in Chun *et al.* (2005). For $St > 0.4$, the model significantly overpredicts the values of c_1. This can be explained if we look at the drift term in (3.4) and how the drift coefficient $A(St)$ depends on St. As St increases beyond 0.4, $\langle S^2 \rangle_p - \langle R^2 \rangle_p$ continues to increase until $St = 0.6$, after which it decreases, but more slowly than the linear prefactor in (3.3), leading to an overall increase in $A(St)$ over the range of Stokes numbers considered. This is inconsistent with the DNS; indeed, the peak c_1 in the DNS occurs at $St \approx 0.7$ and then decreases thereafter. Apparently, the drift-diffusion arguments in Chun *et al.* (2005) are valid for $St \leqslant 0.4$, but beyond that exaggerate the value of c_1 and hence the degree of clustering.

Next we consider the behaviour of w_r in DNS and SPS. The SPS, by construction, is accurate in the limit of $St \to 0$, and we can test this by considering longitudinal structure functions of order p ($S_p(r/\eta, St = 0) = \langle w_r^p(r/\eta, St = 0) \rangle$) for fluid particles. Figure 7 shows structure functions of order $p = 2, 3, 4$ for fluid particles obtained from DNS and SPS. We find excellent quantitative agreement, showing that the SPS correctly captures the limit of $St = 0$. Let us now focus on the second-order structure function S_2 for inertial particles. Figure 8(*a*) shows this quantity for both the DNS and SPS plotted for four different St as a function of r/η. These St are chosen to span the entire range examined and illustrate the fact that, although the qualitative behaviour is very similar, the magnitude of S_2 is not captured by the SPS, except for $St \to 0$. Let us now consider the form

$$S_2(r/\eta, St) = a(St) + b(St)\,(r/\eta)^{\zeta_2}, \tag{3.5}$$

where we allow $S_2(r = 0, St) = a(St)$ to be non-zero owing to inertia-induced caustics (Salazar & Collins 2012). The rate of formation of caustics has been studied theoretically (Duncan *et al.* 2005; Wilkinson *et al.* 2006) and numerically (Falkovich & Pumir 2007) and has been predicted to satisfy an Arrhenius-type expression of the form $a(St) = (\beta^2/3)\exp(-2\alpha/St)$. Salazar & Collins (2012) found reasonably good agreement with this expression, but only for Stokes numbers above a critical value they defined as St_c.

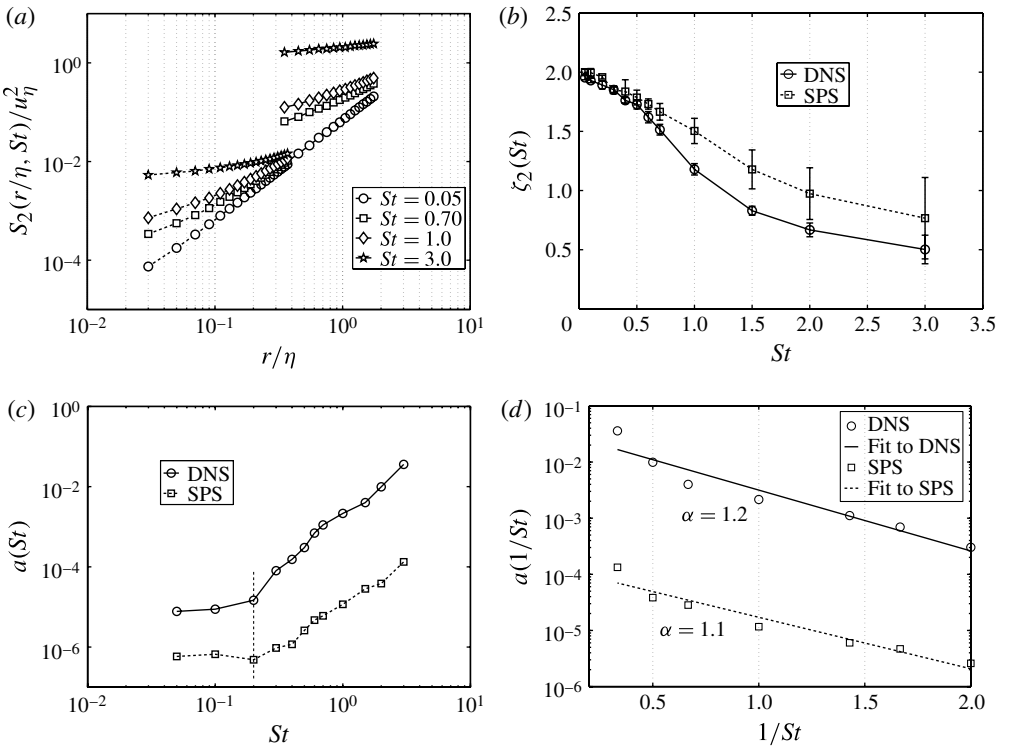

FIGURE 8. (*a*) Variation of S_2 normalized by u_η^2 as a function of r/η for four different St (0.05, 0.70, 1.00 and 3.00) for DNS and SPS: solid lines indicate DNS and dashed lines indicate SPS. (*b*) Variation of ζ_2 as a function of St for DNS and SPS. The error bars correspond to 95 % confidence intervals. (*c*) Variation of $a(St) = S_2(r/\eta = 0, St)$ as a function of St, as obtained from a fit of the form (3.5). (*d*) Comparison of the values of a with the model $a(St) = (\beta^2/3)\exp(-2\alpha/St)$ for DNS and SPS.

We have used nonlinear least squares to compute the coefficients a, b and ζ_2 in (3.5). Figure 8(*c*) shows the activated behaviour of $a(St)$ in our DNS, where the threshold Stokes number St_c is in quantitative agreement with previous results (e.g. Salazar & Collins 2012). More importantly, the SPS captures this activated behaviour and predicts the correct St_c, further affirming that it can capture the physics of particle pair interactions at sub-Kolmogorov scales. However, the magnitude of $a(St)$ is not captured in our SPS, for the reasons discussed previously. In agreement with Salazar & Collins (2012), we find that the caustic activation occurs somewhere between St of 0.2 and 0.5, and we fit the data to the model using a linear least-squares fit for $St \geqslant 0.5$. Figure 8(*d*) shows that both DNS and SPS data fit quite well to the model, with the predicted values of α and β shown in table 2. We can see that the exponential decay law (α) is quite well predicted by both DNS and SPS, in agreement with the values found by Salazar & Collins (2012). Unsurprisingly, the coefficient β representing the magnitude of $a(St)$ is not captured by the SPS. We could now consider the power-law exponent ζ_2. Figure 8(*b*) shows the comparison of ζ_2 obtained from the DNS and the SPS, and we observe good agreement between the two up to $St \approx 0.5$. For larger St, we find that the SPS overpredicts the exponent. We attribute this disagreement to the

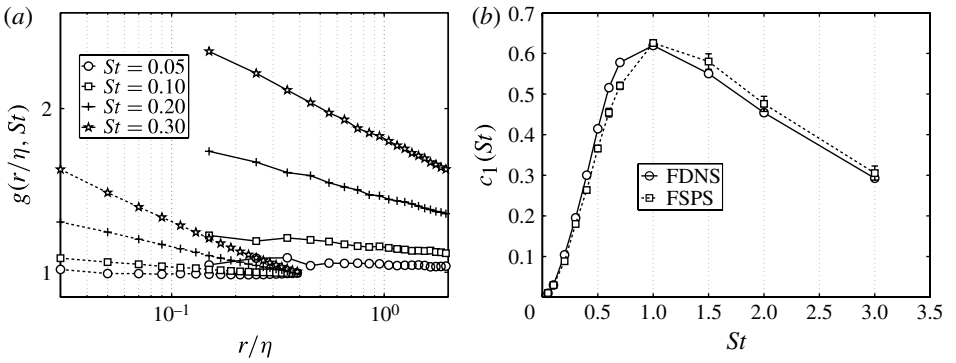

FIGURE 9. (*a*) Variation of the RDF as a function of r/η for four different St (0.05, 0.10, 0.20 and 0.30) in FDNS and FSPS: solid line indicates FDNS and dashed line indicates FSPS. (*b*) Variation of c_1 as a function of St in FDNS and FSPS. The error bars correspond to 95 % confidence intervals.

boundary conditions at $r = R$, which are accurate only for $St \to 0$. This shows that the relative velocity statistics are more sensitive to the effect of the inertial range scales than the RDF.

3.3. *DNS versus SPS: filtered turbulence*

Next we consider the effect of filtering on both the DNS (referred to as FDNS) and SPS (referred to as FSPS). For the FDNS, the fluid velocity is advanced as in an unfiltered DNS and then filtered at every time step for computing the fluid velocity that is used to advance the particle field. In this way, errors due to the filtering do not accumulate in the fluid velocity (we call this *a priori* LES). For the case of the FSPS, the primary inertial particles are advanced by the same algorithm as with the FDNS, the filtered fluid velocity gradient $\tilde{\Gamma}_{ij}^{[p]}(t)$ is computed along the particle trajectory, and this gradient is used to advance the satellite particles. The results for the RDF are given in figure 9. Figure 9(*b*) compares c_1 for the two cases, and we see that there is excellent agreement for $St \leqslant 0.3$ and $St \geqslant 1.0$, with reasonable agreement in between (maximum relative error $\sim$15 %). This shows that, even though a filtered DNS is devoid of the small scales, statistics corresponding to those scales (in this case, the filtered velocity gradient following a primary particle) is sufficient to predict c_1. Furthermore, this demonstrates the utility of the SPS framework for developing and *a priori* testing of LES subgrid models for inertial particles.

We compare the effect of filtering on S_2 in FDNS and FSPS in figure 10. Similar to the unfiltered case, we again observe in figure 10(*a*) that the magnitude of S_2 is not well predicted by the FSPS, except for $St \to 0$. Figure 10(*c*) compares the caustic contribution $a(St)$ (see (3.5)) for DNS, SPS, FDNS and FSPS. We find, quite interestingly, that the caustic activation appears to be delayed as a result of filtering up to $St = 0.4$ as compared to $St = 0.2$ in the DNS. The caustic contribution to the relative velocity can be explained by the 'sling effect' argument of Falkovich & Pumir (2007), whereby energetic uncorrelated vortices in the flow centrifuge out particles with a high velocity that, owing to their inertia, can eventually overlap in space with a finite difference in their velocities. Therefore, caustics are governed by the tails of the p.d.f. of w_r, which are known to be attenuated as a result of filtering (Ray & Collins 2011). Also, the filtered velocity field is devoid of the

Run	α	β/u_η
DNS	1.2	1.9
SPS	1.1	0.1
FDNS	1.6	1.6
FSPS	1.4	0.1
Salazar & Collins (2012) ($R_\lambda = 60$)	1.5	2.8
Salazar & Collins (2012) ($R_\lambda = 120$)	1.2	2.2

TABLE 2. Results from the least-squares fit to $a(St) = (\beta^2/3)\exp(-2\alpha/St)$ for our DNS ($R_\lambda = 95$), SPS, FDNS and FSPS, together with values from Salazar & Collins (2012).

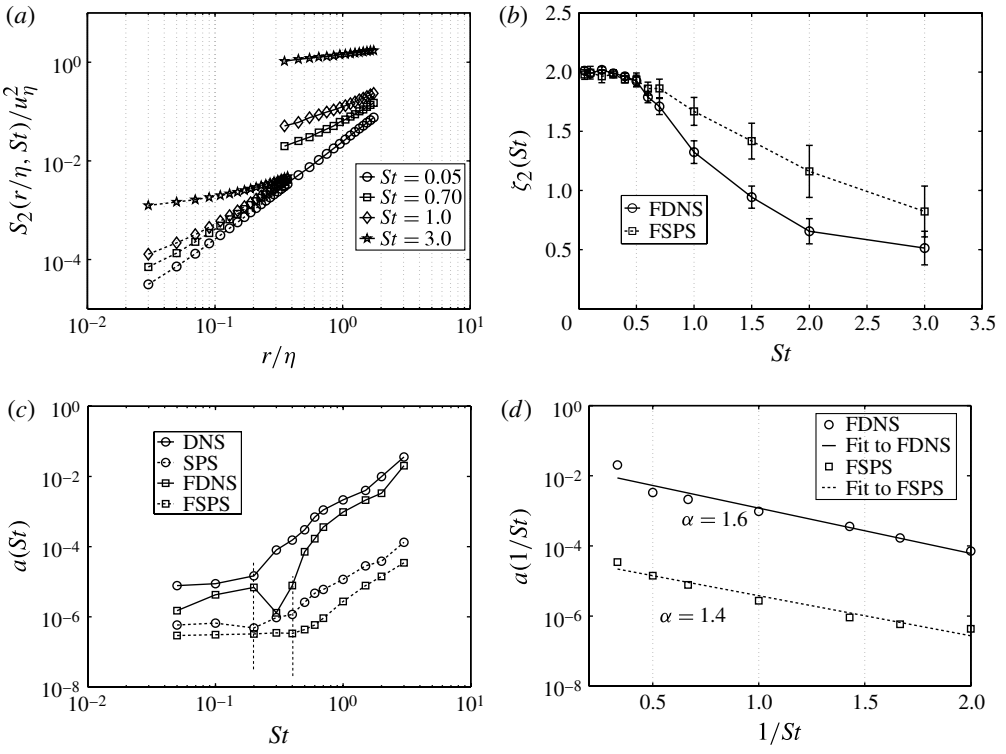

FIGURE 10. (*a*) Variation of S_2 normalized by u_η^2 as a function of r/η for four different St (0.05, 0.70, 1.00 and 3.00) for FDNS and FSPS: solid lines indicate FDNS and dashed lines indicate FSPS. (*b*) Variation of ζ_2 as a function of St for FDNS and FSPS. The error bars correspond to 95 % confidence intervals. (*c*) Variation of the $a(St) = S_2(r/\eta = 0, St)$ as a function of St, as obtained from a fit of the form (3.5) for DNS, SPS, FDNS and FSPS. (*d*) Comparison of the values of a with the model $a(St) = (\beta^2/3)\exp(-2\alpha/St)$ for FDNS and FSPS.

most intense vortices (vortex tubes having a core of characteristic length η) that are present in the unfiltered flow, leading to a weaker sling effect and a consequent delay in the caustic activation. Again, FSPS is able to capture this feature very well. As we did with the unfiltered case, we can compare $a(St)$ with the Arrhenius-type

model $a(St) = (\beta^2/3)\exp(-2\alpha/St)$, and figure 10(*d*) shows that it fits the data well. Table 2 shows the fitted coefficients α and β, indicating that the decay-law α is quite well predicted by FSPS. If we now look at the exponent ζ_2, shown in figure 10(*b*), we see good agreement between FDNS and FSPS for $St \leqslant 0.5$, beyond which the FDNS curve drops off more quickly with St. As mentioned previously, we attribute this discrepancy to the inability of the boundary conditions at $r = R$ in SPS to capture the effect of larger scales on the velocity of newly created satellite particles entering the solution domain.

4. Conclusions

In this paper, we have investigated the behaviour of the radial distribution function (RDF) and the second-order longitudinal velocity structure function S_2 of inertial particles in homogeneous isotropic turbulence using novel satellite particle simulations (SPS). The SPS provides a natural framework for simulating pairwise interaction of particles at the sub-Kolmogorov scales of turbulence, which are essential for predicting the particle collision rates, and very expensive in the framework of a direct numerical simulation (DNS). We have described the concept and implementation of an SPS. We have considered the effect of varying the bounding sphere radius R, and have shown that variations in R/η can be accounted for through simple scaling relations. The SPS, in its current implementation, does not contain any information regarding the larger scales of motion, and consequently cannot predict the magnitude of the RDF. However, it predicts the power-law c_1 of the RDF, in excellent agreement with DNS for St up to 3, indicating that c_1 is determined solely by the small scales. SPS accurately predicts the statistics of w_r in the limit of $St \to 0$, but shows quantitative disagreements at moderate to high St. Specifically, the exponent ζ_2 of S_2 is predicted accurately for $St \leqslant 0.5$. We attribute the disagreement at larger St to the absence of information from the larger scales of motion on the newly created satellite particles entering the simulation domain. The SPS seems to be able to capture the qualitative behaviour of $S_2(r/\eta = 0, St)$, which is known as the caustic contribution to the relative velocity and predicts the rate of 'caustic activation' accurately. We have also considered the effect of filtering and compared FDNS and FSPS, and the findings are very similar to the unfiltered case. We note that the 'caustic activation' seems to be delayed in the filtered velocity field, and attribute this to the attenuation of the tails of the p.d.f. of w_r as a result of filtering. The FSPS predicts c_1 in agreement with FDNS, showing that the SPS can be used to test two-particle LES models for inertial particles designed to recover clustering.

Acknowledgements

This study was supported by the National Science Foundation under grant numbers CBET 0756510 and 0967349. The authors gratefully acknowledge the Texas Advanced Computing Center (TACC) at The University of Texas at Austin for providing HPC resources on Ranger that have contributed to the research results reported within this paper. This work used the Extreme Science and Engineering Discovery Environment (XSEDE), which is supported by National Science Foundation grant number OCI-1053575.

REFERENCES

AHLUWALIA, A. 2002 Preferential concentration of finite Stokes number particles in homogeneous isotropic turbulent flow. PhD thesis, Pennsylvania State University.

AYALA, O., ROSA, B. & WANG, L. P. 2008*a* Effects of turbulence on the geometric collision rate of sedimenting droplets. Part 2. Theory and parameterization. *New J. Phys.* **10**, 075016.

AYALA, O., ROSA, B., WANG, L. P. & GRABOWSKI, W. W. 2008*b* Effects of turbulence on the geometric collision rate of sedimenting droplets. Part 1. Results from direct numerical simulation. *New J. Phys.* **10**, 075015.

BEC, J., BIFERALE, L., CENCINI, M., LANOTTE, A. S. & TOSCHI, F. 2010 Intermittency in the velocity distribution of heavy particles in turbulence. *J. Fluid Mech.* **646**, 527–536.

BINI, M. & JONES, W. P. 2008 Large-eddy simulation of particle-laden turbulent flows. *J. Fluid Mech.* **614**, 207–252.

BRUCKER, K. A., ISAZA, J. C., VAITHIANATHAN, T. & COLLINS, L. R. 2007 Efficient algorithm for simulating homogeneous turbulent shear flow without remeshing. *J. Comput. Phys.* **225**, 20–32.

CHEVILLARD, L. & MENEVEAU, C. 2006 Lagrangian dynamics and statistical geometric structure of turbulence. *Phys. Rev. Lett.* **97**, 174501.

CHUN, J., KOCH, D. L., RANI, S., AHLUWALIA, A. & COLLINS, L. R. 2005 Clustering of aerosol particles in isotropic turbulence. *J. Fluid Mech.* **536**, 219–251.

COLLINS, L. R. & KESWANI, A. 2004 Reynolds number scaling of particle clustering in turbulent aerosols. *New J. Phys.* **6**, 119.

DEVENISH, B. J., BARTELLO, P., BRENGUIER, J.-L., COLLINS, L. R., GRABOWSKI, W. W., IJZERMANS, R. H. A., MALINOWSKI, S. P., REEKS, M. W., VASSILICOS, J. C., WANG, L.-P. & WARHAFT, Z. 2012 Droplet growth in warm turbulent clouds. *Q. J. R. Meteorol. Soc.* **138**, 1401–1429.

DUNCAN, K., MEHLIG, B., ÖSTLUND, S. & WILKINSON, M. 2005 Clustering by mixing flows. *Phys. Rev. Lett.* **95**, 240602.

EATON, J. K. & FESSLER, J. R. 1994 Preferential concentration of particles by turbulence. *Intl J. Multiphase Flow* **20**, 169–209.

FALKOVICH, G., FOUXON, A. & STEPANOV, M. G. 2002 Acceleration of rain initiation by cloud turbulence. *Nature* **419**, 151–154.

FALKOVICH, G. & PUMIR, A. 2007 Sling effect in collisions of water droplets in turbulent clouds. *J. Atmos. Sci.* **64**, 4497.

FEDE, P. & SIMONIN, O. 2006 Numerical study of the subgrid fluid turbulence effects on the statistics of heavy colliding particles. *Phys. Fluids* **18**, 045103.

FESSLER, J. R., KULICK, J. D. & EATON, J. K. 1994 Preferential concentration of heavy particles in a turbulent channel flow. *Phys. Fluids* **6**, 3742–3749.

GIBERT, M., XU, H. & BODENSCHATZ, E. 2012 Where do small, weakly inertial particles go in a turbulent flow? *J. Fluid Mech.* **698**, 160–167.

GRABOWSKI, W. W. & WANG, L.-P. 2012 Growth of cloud droplets in a turbulent environment. *Annu. Rev. Fluid Mech.* **45**, 293–324.

HOGAN, R. C. & CUZZI, J. N. 2001 Stokes and Reynolds number dependence of preferential particle concentration in simulated three-dimensional turbulence. *Phys. Fluids* **13**, 2938–2945.

IRELAND, P. J., VAITHIANATHAN, T., SUKHESWALLA, P. S., RAY, B. & COLLINS, L. R. 2012 Highly parallel particle-laden flow solver for turbulence research. *Comput. Fluids* (in press).

JIN, G., HE, G.-W. & WANG, L.-P. 2010 Large-eddy simulation of turbulent collision of heavy particles in isotropic turbulence. *Phys. Fluids* **22**, 055106.

DE JONG, J., SALAZAR, J. P. L. C., CAO, L., WOODWARD, S. H., COLLINS, L. R. & MENG, H. 2010 Measurement of inertial particle clustering and relative velocity statistics in isotropic turbulence using holographic imaging. *Intl J. Multiphase Flow* **36**, 324–332.

KERSTEIN, A. R. & KRUEGER, S. K. 2006 Clustering of randomly advected low-inertia particles: a solvable model. *Phys. Rev.* E **73**, 025302.

KUERTEN, J. G. M. 2006 Subgrid modeling in particle-laden channel flow. *Phys. Fluids* **18** (2), 025108.

MARCHIOLI, C., SALVETTI, M. V. & SOLDATI, A. 2008 Some issues concerning large-eddy simulation of inertial particle dispersion in turbulent bounded flows. *Phys. Fluids* **20**, 040603.

MAXEY, M. R. 1987 The gravitational settling of aerosol particles in homogeneous turbulence and random flow fields. *J. Fluid Mech.* **174**, 441–465.

MAXEY, M. R. & RILEY, J. J. 1983 Equation of motion for a small rigid sphere in a nonuniform flow. *Phys. Fluids* **26**, 883–889.

MCQUARRIE, D. A. 1976 *Statistical Mechanics*. Harper & Row.

PAN, L. & PADOAN, P. 2010 Relative velocity of inertial particles in turbulent flows. *J. Fluid Mech.* **661**, 73–107.

PATTERSON, G. S. & ORSZAG, S. A. 1971 Spectral calculation of isotropic turbulence: efficient removal of aliasing interactions. *Phys. Fluids* **14**, 2538–2541.

PINSKY, M. B. & KHAIN, A. P. 1997 Turbulence effects on droplet growth and size distribution in clouds – a review. *J. Aerosol Sci.* **28**, 1177–1214.

POZORSKI, J. & APTE, S. V. 2009 Filtered particle tracking in isotropic turbulence and stochastic modeling of subgrid-scale dispersion. *Intl J. Multiphase Flow* **35**, 118–128.

RAY, B. & COLLINS, L. R. 2011 Preferential concentration and relative velocity statistics of inertial particles in Navier–Stokes turbulence with and without filtering. *J. Fluid Mech.* **680**, 488–510.

READE, W. C. & COLLINS, L. R. 2000*a* Effect of preferential concentration on turbulent collision rates. *Phys. Fluids* **12**, 2530–2540.

READE, W. C. & COLLINS, L. R. 2000*b* A numerical study of the particle size distribution of an aerosol undergoing turbulent coagulation. *J. Fluid Mech.* **415**, 45–64.

SALAZAR, J. P. L. C. & COLLINS, L. R. 2012 Inertial particle relative velocity statistics in homogeneous isotropic turbulence. *J. Fluid Mech.* **696**, 45–66.

SALAZAR, J. P. L. C., DE JONG, J., CAO, L., WOODWARD, S., MENG, H. & COLLINS, L. R. 2008 Experimental and numerical investigation of inertial particle clustering in isotropic turbulence. *J. Fluid Mech.* **600**, 245–256.

SAW, E. W., SHAW, R. A., AYYALASOMAYAJULA, S., CHUANG, P. Y. & GYLFASON, A. 2008 Inertial clustering of particles in high-Reynolds-number turbulence. *Phys. Rev. Lett.* **100**, 214501.

SHAW, R. A. 2003 Particle–turbulence interactions in atmospheric clouds. *Annu. Rev. Fluid Mech.* **35**, 183–227.

SHAW, R. A., READE, W. C., COLLINS, L. R. & VERLINDE, J. 1998 Preferential concentration of cloud droplets by turbulence: effects on the early evolution of cumulus cloud droplet spectra. *J. Atmos. Sci.* **55**, 1965–1976.

SHOTORBAN, B. & MASHAYEK, F. 2005 Modeling subgrid-scale effects on particles by approximate deconvolution. *Phys. Fluids* **17**, 081701.

SHOTORBAN, B. & MASHAYEK, F. 2006*a* On stochastic modeling of heavy particle dispersion in large-eddy simulation of two-phase turbulent flow. In *IUTAM Symposium on Computational Multiphase Flow*, pp. 373–380. Springer.

SHOTORBAN, B. & MASHAYEK, F. 2006*b* A stochastic model for particle motion in large-eddy simulation. *J. Turbul.* **7**, N11.

SQUIRES, K. D. & EATON, J. K. 1991 Preferential concentration of particles by turbulence. *Phys. Fluids* A **3**, 1169–1178.

SUNDARAM, S. & COLLINS, L. R. 1997 Collision statistics in an isotropic, particle-laden turbulent suspension. Part I. Direct numerical simulations. *J. Fluid Mech.* **335**, 75–109.

SUNDARAM, S. & COLLINS, L. R. 1999 A numerical study of the modulation of isotropic turbulence by suspended particles. *J. Fluid Mech.* **379**, 105–143.

WANG, L. P. & MAXEY, M. R. 1993 Settling velocity and concentration distribution of heavy particles in homogeneous isotropic turbulence. *J. Fluid Mech.* **256**, 27–68.

WANG, L.-P., WEXLER, A. S. & ZHOU, Y. 2000 Statistical mechanical description and modeling of turbulent collision of inertial particles. *J. Fluid Mech.* **415**, 117–153.

WILKINSON, M., MEHLIG, B. & BEZUGLYY, V. 2006 Caustic activation of rain showers. *Phys. Rev. Lett.* **97**, 048501.

WITKOWSKA, A., BRASSEUR, J. G. & JUVÉ, D. 1997 Numerical study of noise from isotropic turbulence. *J. Comput. Acoust.* **5**, 317–336.

ZAICHIK, L. I. & ALIPCHENKOV, V. M. 2007 Refinement of the probability density function model for preferential concentration of aerosol particles in isotropic turbulence. *Phys. Fluids* **19** (11), 113308.

ZAICHIK, L. I. & ALIPCHENKOV, V. M. 2009 Statistical models for predicting pair dispersion and particle clustering in isotropic turbulence and their applications. *New J. Phys.* **11**, 103018.

ZEMACH, C. 1998 Appendix A: Mathematics of fluid mechanics. In *The Handbook of Fluid Dynamics* (ed. R. W. Johnson). CRC Press.